Bulletin of Earth Sciences of Thailand

Fold characteristics and deformation styles within fold and thrust belts using 2D numerical modelling

Wasin Meesuay[1, *], Sukonmeth Jitmahantakul[1,2] and Raphael Bissen[2,3]

1. Department of Geology, Faculty of Science, Chulalongkorn University, Bangkok 10330, Thailand
2. Basin Analysis and Structural Evolution Research Unit (BASE RU), Department of Geology, Faculty of Science, Chulalongkorn University, Bangkok 10330, Thailand
3. Department of Mining and Petroleum Engineering, Faculty of Engineering, Chulalongkorn University, Bangkok 10330, Thailand

*Corresponding Author: meesuay.wasin@gmail.com

Received: 21 Jun 2022
Revised: 21 Jul 2022
Accepted: 21 Jul 2022

Abstract

This study used Discrete Element Modelling (DEM) to simulate the two-dimensional structural deformation within fold and thrust belts that are associated with plate collision. A total of 12 models were performed with different basal inclinations and pre-kinematic thickness. The results reveal that the thrust-related structures are dominated by pop-up structure and triangle zone. These structures commonly exhibit a kink band style folding in the hanging wall. The location of the active frontal fold, fold spacing, and fold types are controlled by pre-kinematic thickness. Thicker models are characterized by box-type folds, while thinner models are characterized by chevron-type folds. Hence, the difference in the pre-kinematic thickness will have a significant impact on the folding structure, while the basal inclination has no effect based on our structural analysis.

Keywords : Fold and Thrust Belt, Discrete Element Modelling, Pre-Kinematic Thickness, Basal Inclination, Numerical Sandbox Modelling

1. Introduction

The term fold and thrust belt (FATB) refers to a compression zone that is associated with plate collision. It can also be applied to the gravitation-induced compressional zone in the passive margins, e.g. the Gulf of Mexico and Niger Delta (Morley et al., 2011; Poblet and Lisle, 2011; Yang et al., 2020). FATB settings hold major oil and gas fields, such as the Zagros FATB of Iran in the Middle East. The complexity of the fold and thrust systems in the FATB region poses significant challenges for exploration geologists. Understanding thrust-related fold styles and evolution within FATBs is important for seismic interpretation of structural traps.

Formerly, scaled physical modeling of the compressional wedge was used to simulate structural deformation within FATB. There are various factors that affect the structural styles of the FATBs. These factors include basal décollement, deforming material, and convergence kinetics (Graveleau et al., 2012). Generally, physical sandbox modelling experiments are limited by the tools and materials used, which will be very painful for replicating the experiments. Otherwise, recent studies have shown the essentials of numerical modeling techniques in structural analysis of crustal deformation by using Discrete Element Modelling (DEM) technique to create 'numerical sandbox modelling' (Benesh et al., 2007; Dean et al., 2015; Dean et al., 2013; Finch and Gawthorpe, 2017; Hardy, 2018, 2019; Hardy and Finch, 2005, 2007; Hardy et al., 2009; Li et al., 2020; Meng and Hodgetts, 2019a, b; Morley et al., 2011; Ruh et al., 2012; Zhang, 2012; Zhang et al., 2020).

DEM is a technique of numerical modelling involves creating different number of small particles under different conditions. These particles, created in the models, can replace the sand particles used in sandbox modelling. Unlike other numerical modelling technique, such as Finite Element Modelling (FEM) which normally used to work in static or low strain conditions, DEM is very useful to simulate the high strain conditions such as fault and fold structure development in geology. This technique allows inter-particle dynamics and the high strain structural features to be simulated, visualized, and analyzed in computer without preparing any physical setup. For example, Meng and Hodgetts (2019a) revealed that the rate of deformation was the inverse of the cover rock layer cohesion and the decollement layer thickness had direct effect on the amplitude and surface uplift based on DEM. Moreover, Morgan (2015) found that the increase in the cohesion resulted in a substantial increase in the fault offset and fault spacing. Therefore, this study used DEM to simulate the two-dimensional structural deformation within FATBs with different basal inclinations and pre-kinematic thickness. Quantitative analysis of thrust-related folds was performed to characterize fold types and structural styles in a compressional zone.

2. Methodology

2.1 General setup

Computational experiments (Fig. 1) were set up and run by using ESyS-Particle, which is an open-source software for particle-based numerical modelling.

The model setup composed of three invisible walls on the left, right, and bottom sides. The bottom and right walls were fixed and acted as the boundaries to stop the particles from moving out of the simulation area. Experiment was initiated by moving the left wall at a very slow constant speed (2.5 mm/s), to maintain the models under quasi-static condition, from left to right. The experiment was stopped when the total shortening rate reached 50 percent.

2.2 Model particles and scaling

Model particles were composed of rotating 2D spheres. They were arranged in poorly-sorted configuration with a radius of around 0.3-1.5 mm in an enclosed rectangular box of 800 mm in length. All simulation models were downscaled to 10^5 times smaller than the natural prototypes. This scaling factor is a general spatial scaling that has been found to be suitable in previous analogue modelling experiments (McClay, 1990; McClay and White, 1995).

2.3 Model stratigraphy

In each model, there are two mechanically-different units. The first unit is 5 mm thick representing a décollement layer in FATBs, which is cohesionless and frictionless (Fig. 1). This unit is rheologically equivalent to overpressured shale or salt layer in the natural prototype. It is colored as blue in the model.

The second unit consists of cohesive layers, shown as red-white layers in the model (Fig. 1), where particles are bonded by the brittle-beam interaction law and behave like crustal rocks. The values of four mandatory parameters (Young's modulus, Cohesion strength, Poisson's ratio, and internal angle of friction) applied in the models are shown in Table 1.

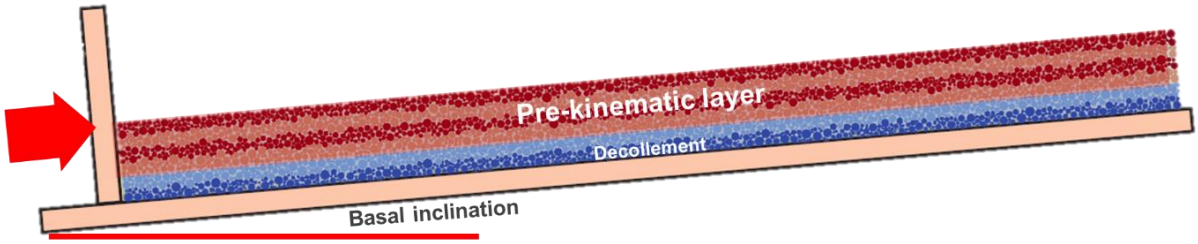

Figure 1 Experimental setup for 2D inclined DEM modelling. The left wall pushes the pre-kinematic unit (red layers) and the underlying décollement unit (blue layers) to the right (as indicated by the red arrow). Basal inclination is measured from horizontal.

Table 1 Parameters of particle and interaction of each layer

Layers	Density (kg/m^3)	Prototype Equivalent Young's Modulus (GPa)	Prototype Equivalent Cohesion Strength (MPa)	Internal Angle of Friction	Poisson's Ratio	Static / Dynamic Frictional Coefficient
Pre- kinematic	2500	5	20	16.7	0.25	0.3/0.1
Décollement	2200	0	0	0	0.4	0/0

Faults develop when the compressional force breaks the bond and particles enter the frictional mode. The package's cohesive layer is composed of 5 GPa Young's modulus, 20 MPa Cohesion strength, and a 16.7-degree internal angle of friction. The values in Table 1, including the density, Young's modulus, cohesion strength, Poisson's ratio, internal angle of friction, static and dynamic frictional coefficient, are derived from the previous studies (Dean et al., 2015; Dean et al., 2013; Hardy and Finch, 2005; Morgan, 2015; Li et al., 2020; and Zhang, 2012) to represent the general Earth's upper crustal properties.

2.4 Simulation process

The model workflow is summarized in Figure 2. It began with parameter validation (Fig. 3). This process involved performing compressional biaxial testing to ensure that the macroscopic parameters were consistent with the microscopic parameters of the grain package assigned in section 2.3. The compressional biaxial testing was performed by moving walls in all directions to the rectangular 60mm x 80mm particle package (Fig. 3a). Additional parameters, such as the damping and gravity, were also analyzed. The snapshot details of the wall parameters, such as interacted force and stress, were also captured to record the stress development in different stress load through times (Fig. 3b). Brittle failure observed in the calibration process was comparable with brittle deformation of typical granitic crustal rocks.

After calibrating the parameters, the full initial geometry of particle packages (enclosed rectangular box of 800 mm length as mentioned in the model stratigraphy) was constructed, and then was inserted into the script of full simulation. The entire simulation took around four to eight hours. It was performed with twelve cores and a processing speed of 2.4 GHz CPU.

In this study, two main factors, basal inclination and initial thickness of pre-kinematic layers (Fig. 3) vary with

three different initial layer thickness (20, 40, 60 mm thickness) and four different basal inclination (0, 2, 4, 6 hinterlands dipping degree) were paired and simulated. The total numbers of simulations were 12 models.

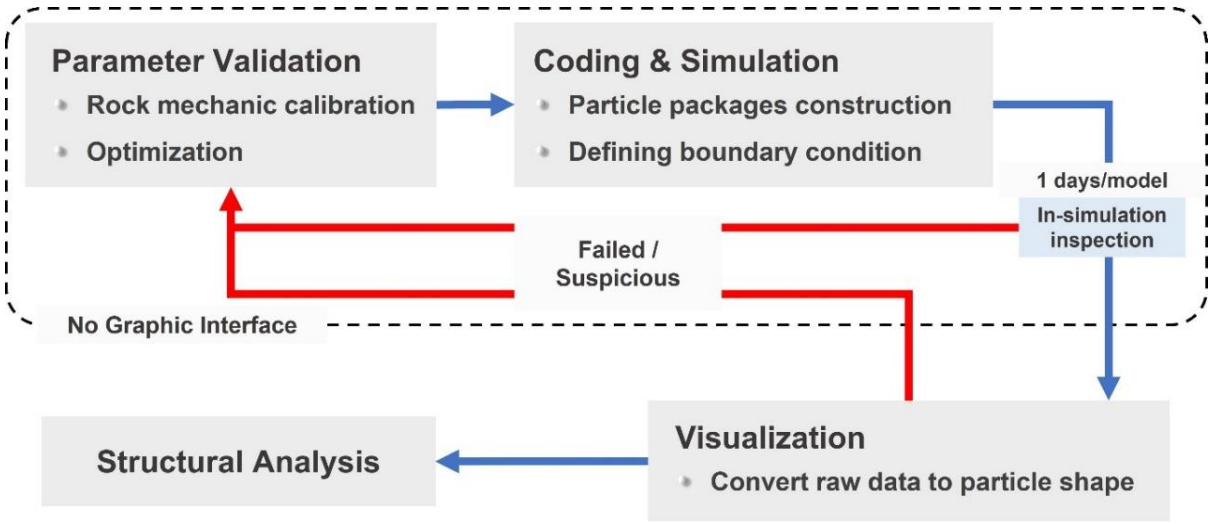

Figure 2 Diagram showing the workflow of DEM used in this study. Parameter validation and simulation processes were performed using ESyS-Particle. Model results were visualized for quantitative fold analysis.

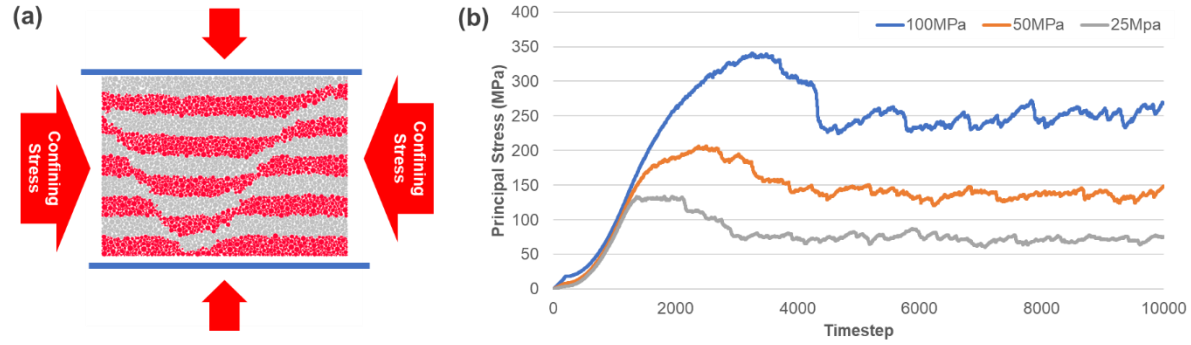

Figure 3 (a) Particle package underwent compressional biaxial testing for parameters calibration. (b) Graph showing stress development in each individual confining stress through times. The stress shows a brittle behavior, which is composed of elastic zone (linear stress pile-up) and small plastic zone (curvy top), before entering to failure zone. This behavior is also typically found in brittle rock in natural prototype.

After the simulation process was completed, the snapshots of each deformation step were converted to .vtk files, which are commonly used for visualization. The vtk files were opened by the ParaView software to visualize the results of the simulation. This open-source program is acceptable for scientific and technical applications. A series of deformation images was interpreted and analyzed.

3. Results

A total of 12 models were performed with different basal inclinations

and pre-kinematic thickness (Figs. 4 - 7). These models were grouped into two model series: pre-kinematic thickness models (PTMS) and inclined model series (IMS).

3.1 Pre-kinematic thickness model series (PTMS)

The goal of this model series is to understand the effects of pre-kinematic thickness on FATB. There were two model sets: the first set had 0-degree basal inclination (Fig. 4) and the second set ran with 6-degree basal inclination (Fig. 5). Each set consisted of three models that had varying pre-kinematic thickness.

The results show that the number of folds decreases as the pre-kinematic thickness increases (Fig. 8a). For example, the number of folds decreased from 8 to 4-6 (25-50% decrease) when the pre-kinematic layer thickness is increased from 20 to 60 mm (100-200% increase) (Fig. 8a). The locations of active frontal folds are also influenced by the increase of pre-kinematic thickness. For example, the active frontal fold occurs farther from the moving wall when the pre-kinematic layer is increased (530-550 mm from the moving wall in Model A1 and A4, 800 mm in Model C1 and C4) (Figs. 4 -5). The increasing pre-kinematic thickness also contributes to the increase in the folding wavelength.

3.2 Inclined model series (IMS)

The goal of this model series is to understand the effects of basal inclination on FATB structures. There were two model sets based on the thickness of the pre-kinematic layers: thin (20 mm; C1 – C4; Fig. 6) and thick (60 mm; A1-A4; Fig. 7) models. The results show that basal inclination is less likely to affect the structural styles of folding and the number of folds (Figs. 6-7).

4. Quantitative fold analysis

In order to characterize the fold types in FATB models, the quantitative analysis was performed by numeric measurement of fold geometry based on Hudleston (1973) fold classification. This is because it allows the folding structure to be described quantitatively in terms of the amplitudes of the fold quarter (D3) and quarter of the folding wavelength (W) (Hudleston, 1973). The measurement of these parameters was performed in the layer that is 10 mm above the décollement unit.

The measurement results can be divided into two categories: W and D3. The W of all models ranges from near zero to almost 40 mm, while the D3 in the range of 0-20 mm. Cross plots between these measurements show similar distribution in PTMS (Fig. 9a) and IMS (Fig. 10a), which imply that folding structures develop in the same size. However, the visual interpretation suggested that the fold would grow bigger when pre-kinematic thickness was increased. When considering carefully, the visual interpretation is counting the fold size in terms of the regional overview, however, the measurement involved only the layer 10 mm above the décollement unit. Hence, this can help to explain that, in our models, the increasing pre-kinematic thickness grows the fold size by enlarging the stretched outer arc zone.

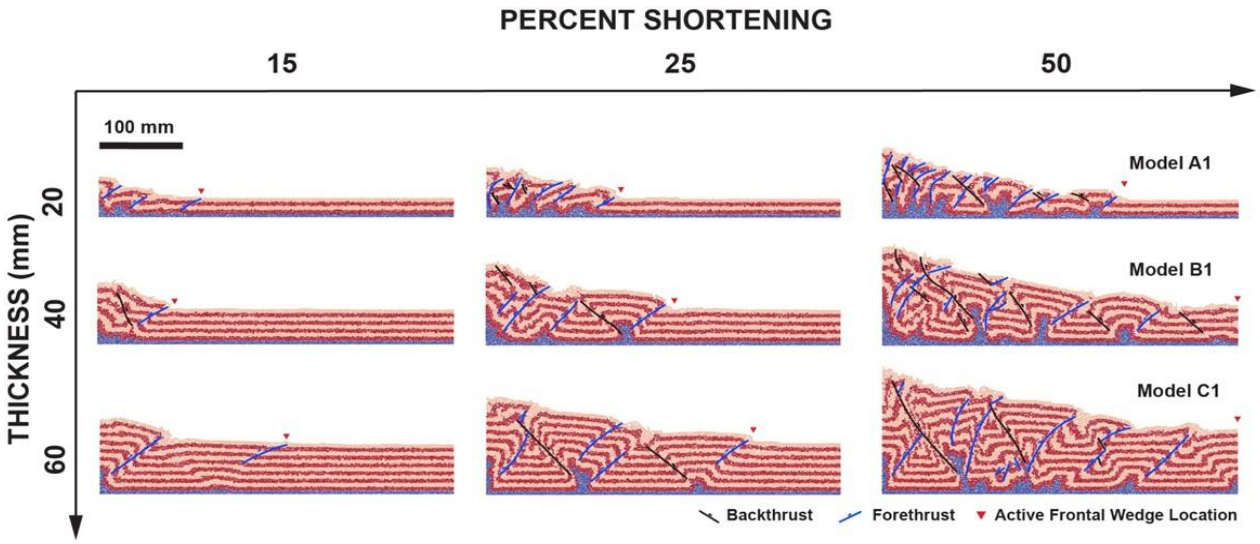

Figure 4 Comparison of 0-degree basal inclination PTMS (models A1, B1 and C1) at 15, 25 and 50 percent shortening. The number of folds decreases with the increasing of pre-kinematic thickness. The active frontal fold (red triangle) occurs farther from the moving wall when the pre-kinematic layer is increased.

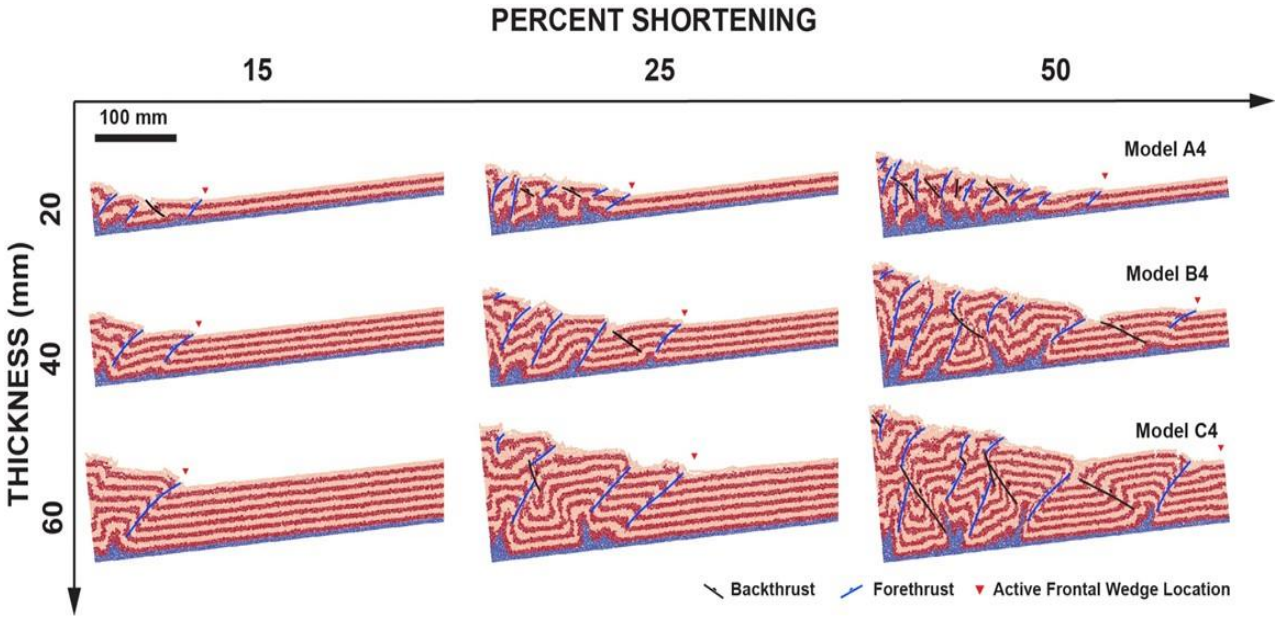

Figure 5 Comparison of 6-degree basal inclination PTMS (models A4, B4 and C4) at 15, 25 and 50 percent shortening. Both the number of folds and the active frontal fold location tends to have the same trends with no basal inclination PTMS models when the pre-kinematic thickness increased.

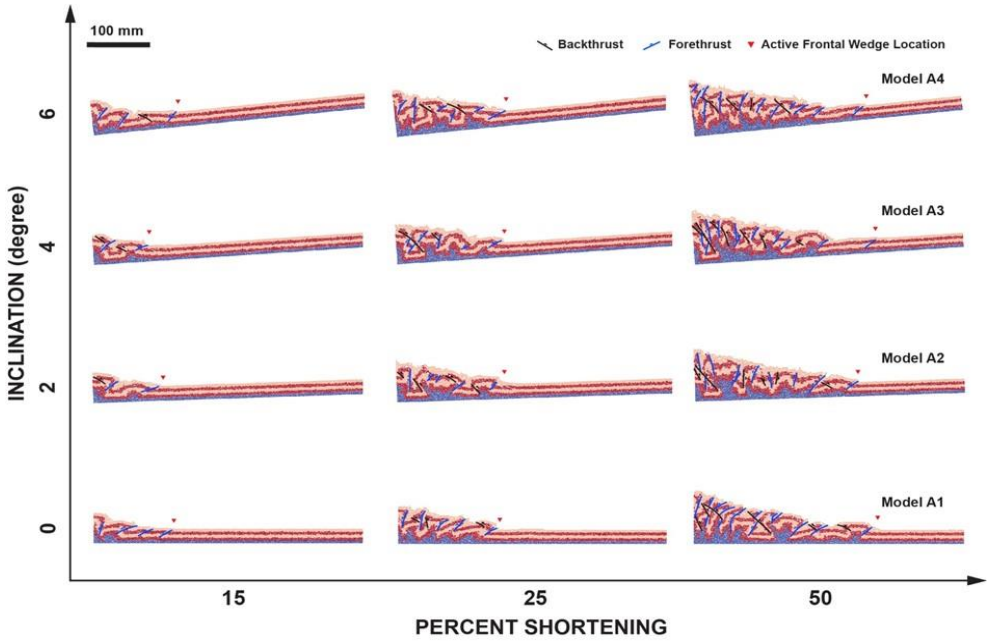

Figure 6 Comparison of thin IMS (models A1, A2, A3 and A4) at 15, 25 and 50 percent shortening. The number of folds and the location of active frontal fold are similar in all models. The change of basal inclination is likely having no effects on folding styles.

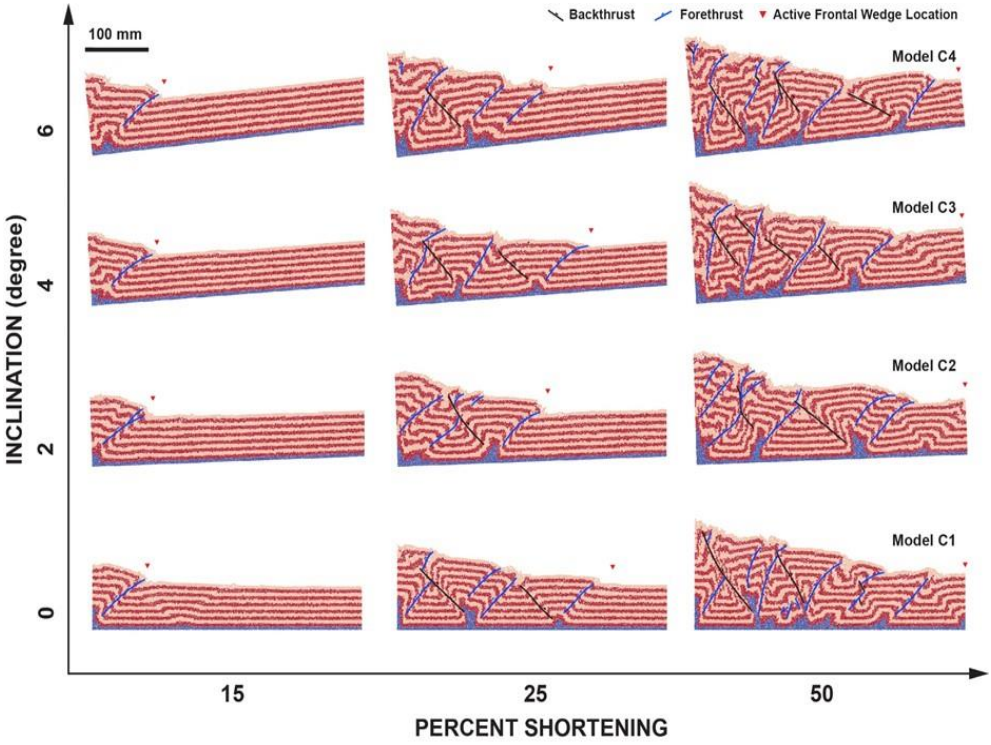

Figure 7 Comparison of thick IMS (models C1, C2, C3 and C4) at 15, 25 and 50 percent shortening. The thick IMS models show lower number of deformation structure than the thin IMS and the basal inclination show less effects on models as same as the thin IMS suite.

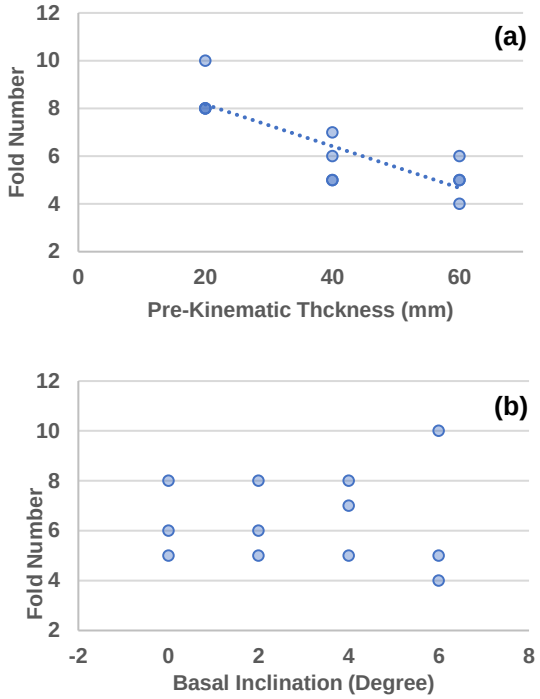

Figure 8 Fold number plots when considered along with (a) pre-kinematic thickness of models and (b) initial basal inclination of models. The fold number shows a negative correlation pattern with the pre-kinematic thickness: the increase of pre-kinematic thickness will decrease the fold number occurring in the model. When considering the fold number with the basal inclination, there is no obvious relationship in the plot.

In order to complete the plot of Huddleson (1973), these two parameters need to be derived into 'B1' (relative amplitude factors) and B3 (chevron - box folding indicator), based on Fourier's transformation. This implied to the relative amplitude and bluntness-sharpness of fold. The results were grouped and presented according to PTMS (Fig. 9b) and IMS (Fig. 10b).

The PTMS suite shows difference in the distribution of the fold. Thicker models are characterized by box-type folds, while thinner models are characterized by chevron-type folds. On the other hand, the scatter plots show that the IMS seems not to have any difference on the data distribution (Fig. 10b). Hence, this can conclude that the basal inclination does not affect the folding structural styles.

The resutls presented in this study are in agreement with previous analog and numerical modelling studies (Huiqi et al., 1992; Soto et al., 2002; Dean et al., 2015). Analog modelling performed by Huiqi et al. (1992) and Soto et al. (2002) found the same relationship as this study that the increase in the layer thickness resulted in the reduction of the number of folds. Dean et al. (2015) studied the same factors as this study, but in the gravity-induced compressional system. This study is in agreement with Dean et al. (2015) that the increase in layer thickness implies to the increase in the deformation structure spacing. However, Dean et al. (2015) did not mention the effect of basement inclination on the folding structure.

5. Conclusion

DEM models of compressional setting illustrate the effects of pre-kinematic thickness and basement inclination on thrust-related folds. The pre-kinematic thickness affects the frequency and size of the fold in models.

In thinner models, the fold type is more prominent on the endmembers of the box-type ends, while in thinner models, the fold type is more prominent on the chevron-type endmembers. Although the basal inclination of the models has low effect on the folds, the difference in the thickness of the side will have a significant impact on the folding.

As our study shows that the pre-kinematic thickness affects folding structure, this can be a reference for future FATB studies focusing on thin crustal layer, such as subduction zones, or thick crustal layer (e.g., orogenic belts). Also, this can be extended to cover FATB with different deposition rate. Our result shows

the parallel conclusion with Wu and McClay (2011) that the thick layer (high sedimentation) is likely to have a wide spacing of deformation while low sedimentation shows a close spacing deformation.

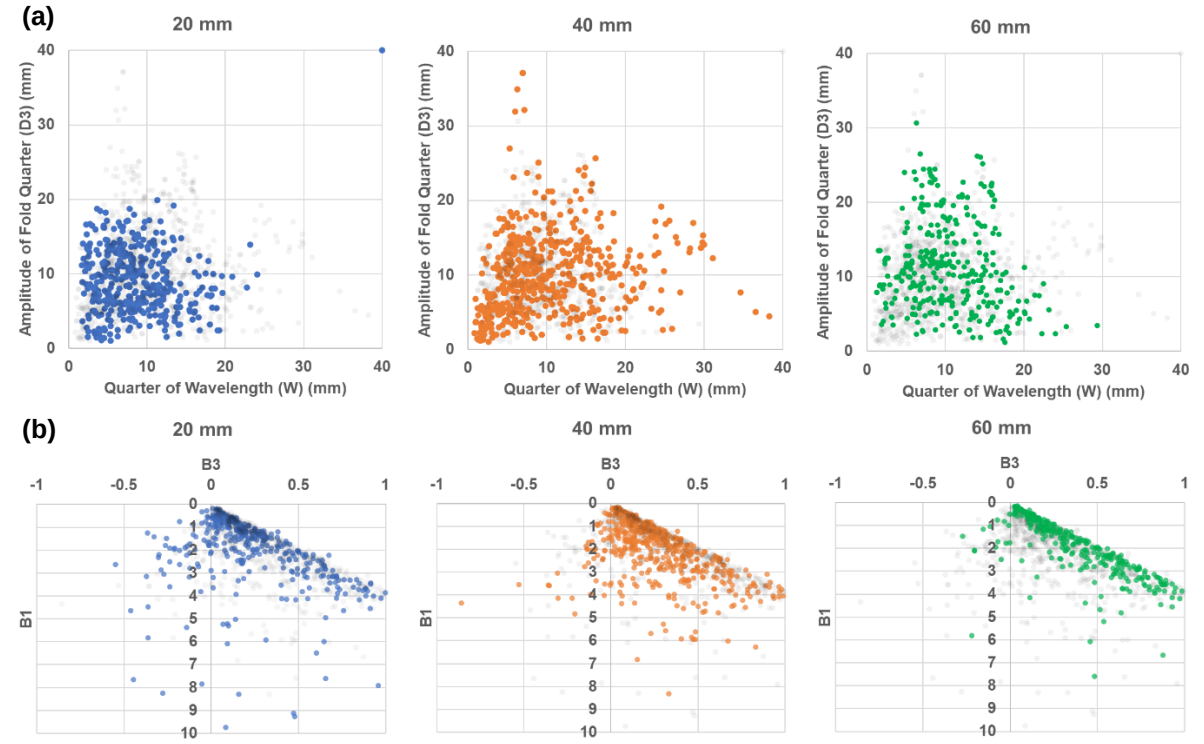

Figure 9 (a) Cross-plot of the quarter of wavelength of folds (W) with the amplitudes of the fold quarter (D3). Both of them are mostly under 20 mm. **(b)** Fold classification plot after Hudleston (1973) using B1 (relative amplitude) and B3 (chevron - box folding) parameters. All data are grouped by pre-kinematic thickness. The data falls in part of 'chevron folding' (left) for the 20 mm thickness, while the thicker pre-kinematic thickness shows less portion of data fall into left side.

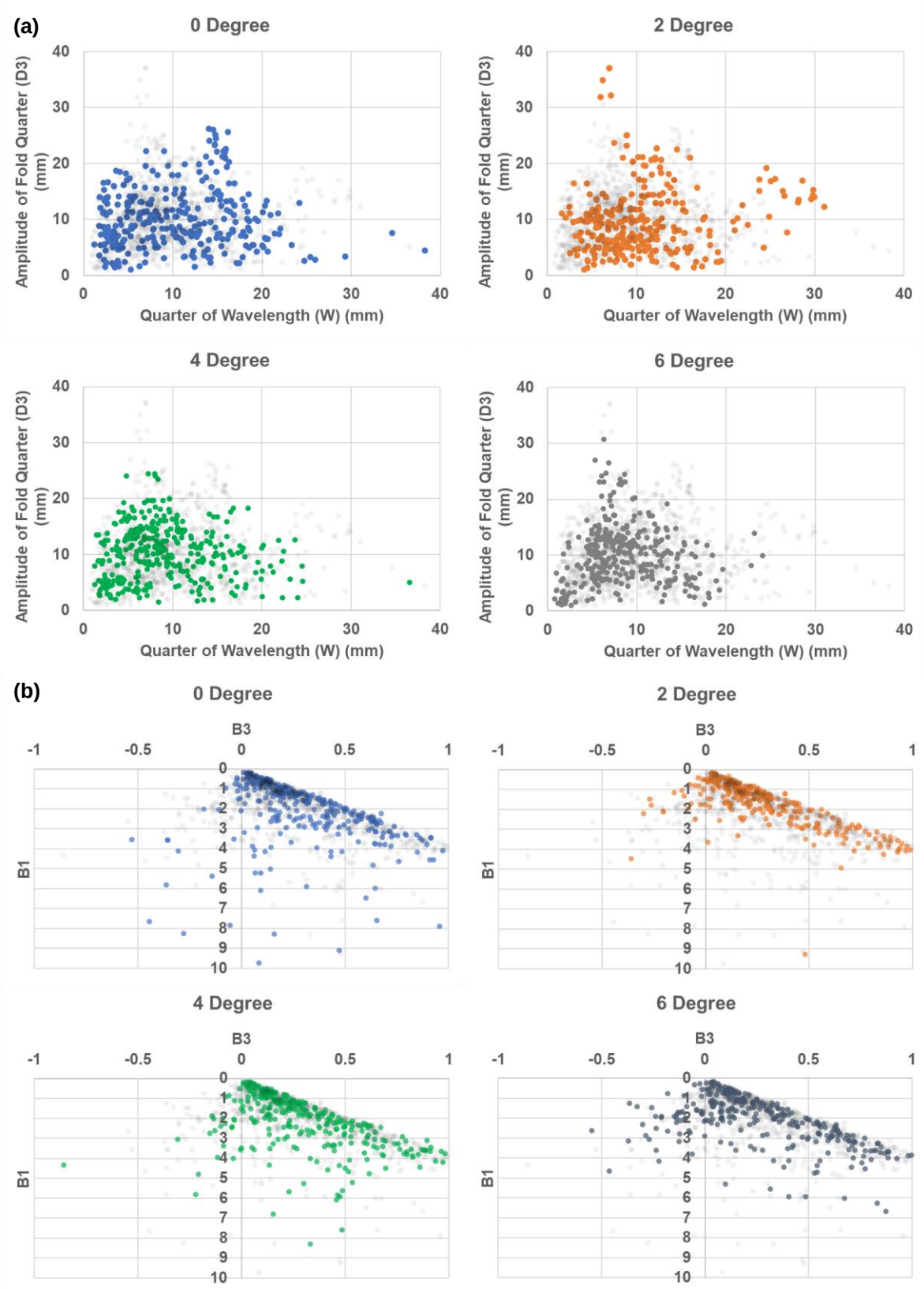

Figure 10 (a) Cross-plot of the quarter of wavelength of folds (W) with the amplitudes of the fold quarter (D3). Both of them are mostly under 20 mm. **(b)** Fold classification plot after Hudleston (1973) using B1 (relative amplitude) and B3 (chevron - box folding) parameters. The scatters plot show that the data with basal inclination grouping seems not to have any difference on the data distribution.

6. Acknowledgement

The M.Sc. Petroleum Geoscience Program at Department of Geology, Faculty of Science, Chulalongkorn University is thanked for providing a workstation that allows authors to simulate models.

7. References

Benesh, N. P., Plesch, A., Shaw, J. H., and Frost, E. K., 2007, Investigation of growth fault bend folding using discrete element modeling: Implications for signatures of active folding above blind thrust faults: Journal of Geophysical Research: Solid Earth, v. 112, no. B3.

Dean, S., Morgan, J., and Brandenburg, J. P., 2015, Influence of mobile shale on thrust faults: Insights from discrete element simulations: AAPG Bulletin, v. 99, no. 3, p. 403-432.

Dean, S. L., Morgan, J. K., and Fournier, T., 2013, Geometries of frontal fold and thrust belts: Insights from discrete element simulations: Journal of Structural Geology, v. 53, p. 43-53.

Finch, E., and Gawthorpe, R., 2017, Growth and interaction of normal faults and fault network evolution in rifts: insights from three-dimensional discrete element modelling: Geological Society, London, Special Publications, v. 439, no. 1, p. 219.

Graveleau, F., Malavieille, J., and Dominguez, S., 2012, Experimental modelling of orogenic wedges: A review: Tectonophysics, v. 538-540, p. 1-66.

Hardy, S., 2018, Coupling a frictional-cohesive cover and a viscous substrate in a discrete element model: First results of application to thick- and thin-skinned extensional tectonics: Marine and Petroleum Geology, v. 97, p. 32-44.

-, 2019, Discrete element modelling of extensional, growth, fault-propagation folds: Basin Research, v. 31, no. 3, p. 584-599.

Hardy, S., and Finch, E., 2005, Discrete-element modelling of detachment folding: Basin Research, v. 17, no. 4, p. 507-520.

-, 2007, Mechanical stratigraphy and the transition from trishear to kink-band fault-propagation fold forms above blind basement thrust faults: A discrete-element study: Marine and Petroleum Geology, v. 24, no. 2, p. 75-90.

Hardy, S., McClay, K., and Anton Muñoz, J., 2009, Deformation and fault activity in space and time in high-resolution numerical models of doubly vergent thrust wedges: Marine and Petroleum Geology, v. 26, no. 2, p. 232-248.

Hudleston, P. J., 1973, Fold morphology and some geometrical implications of theories of fold development: Tectonophysics, v. 16, no. 1, p. 1-46.

Huiqi, L., McClay, K. R., and Powell, D., 1992, Physical models of thrust wedges, *in* McClay, K. R., ed., Thrust Tectonics: Dordrecht, Springer Netherlands, p. 71-81.

Li, J., Zhang, Y., Wang, H., and Wang, D., 2020, Three-dimensional discrete element numerical simulation of Paleogene salt structures in the western Kuqa foreland thrust belt: Petroleum Exploration and Development, v. 47, no. 1, p. 68-79.

McClay, K. R., 1990, Deformation mechanics in analogue models of extensional fault systems: Geological Society, London, Special Publications, v. 54, no. 1, p. 445.

McClay, K. R., and White, M. J., 1995, Analogue modelling of orthogonal and oblique rifting: Marine and Petroleum Geology, v. 12, no. 2, p. 137-151.

Meng, Q., and Hodgetts, D., 2019a, Combined control of décollement layer thickness and cover rock cohesion on structural styles and evolution of fold belts: A discrete element modelling study: Tectonophysics, v. 757, p. 58-67.

-, 2019b, Structural styles and decoupling in stratigraphic sequences with double décollements during thin-skinned contractional tectonics: Insights from numerical modelling: Journal of Structural Geology, v. 127, p. 103862.

Morgan, J. K., 2015, Effects of cohesion on the structural and mechanical evolution of fold and thrust belts and contractional wedges: Discrete

element simulations: Journal of Geophysical Research: Solid Earth, v. 120, no. 5, p. 3870-3896.
Morley, C. K., King, R., Hillis, R., Tingay, M., and Backe, G., 2011, Deepwater fold and thrust belt classification, tectonics, structure and hydrocarbon prospectivity: A review: Earth-Science Reviews, v. 104, no. 1, p. 41-91.
Poblet, J., and Lisle, R. J., 2011, Kinematic evolution and structural styles of fold-and-thrust belts: Geological Society, London, Special Publications, v. 349, no. 1, p. 1.
Ruh, J. B., Kaus, B. J. P., and Burg, J.-P., 2012, Numerical investigation of deformation mechanics in fold-and-thrust belts: Influence of rheology of single and multiple décollements: Tectonics, v. 31, no. 3.
Soto, R., Casas, A. M., Storti, F., and Faccenna, C., 2002, Role of lateral thickness variations on the development of oblique structures at the Western end of the South Pyrenean Central Unit: Tectonophysics, v. 350, no. 3, p. 215-235.
Wu, J. E., and McClay, K. R., 2011, Two-dimensional Analog Modeling of Fold and Thrust Belts: Dynamic Interactions with Syncontractional Sedimentation and Erosion, *in* McClay, K., Shaw, J., and Suppe, J., eds., Thrust Fault-Related Folding, Volume 94, American Association of Petroleum Geologists, p. 0.
Yang, X., Peel, F. J., McNeill, L. C., and Sanderson, D. J., 2020, Comparison of fold-thrust belts driven by plate convergence and gravitational failure: Earth-Science Reviews, v. 203, p. 103136.
Zhang, T., 2012, Numerical modelling of deformation within accretionary prisms.
Zhang, Y., Li, J., Lei, Y., Yang, M., and Cheng, P., 2020, 3D simulations of salt tectonics in the Kwanza Basin: Insights from analogue and Discrete-Element numerical modeling: Marine and Petroleum Geology, v. 122, p. 104666.